UNIVERSITY OF PARDUBICE

FACULTY OF CHEMICAL TECHNOLOGY

Institute of Environmental and Chemical Engineering

MSc. Oleksandr Matvieiev

Novel screen-printed sensors with boron-doped diamond electrode: preparation, characterization, modification, and application in electroanalysis

Theses of the Doctoral Dissertation

Pardubice 2024

Study program: **Chemical and Process Engineering**

Study field: **Environmental Engineering**

Author: **MSc. Oleksandr Matvieiev**

Supervisor: **Doc. Ing. Renáta Šelešovská, Ph.D.**

Year of the defense: 2024

Reference
MATVIEIEV, Oleksandr. Novel screen-printed sensors with boron-doped diamond electrode: preparation, characterization, modification, and application in electroanalysis. Pardubice, 2024. Dissertation thesis (Ph.D.). University of Pardubice, Faculty of Chemical Technology, Institute of Environmental and Chemical Engineering, Supervisor doc. Ing. Renáta Šelešovská, Ph.D.

Abstract
This Ph.D. thesis involved the preparation of new screen-printed sensors (SPE) with chemically deposited boron-doped diamond electrode (BDDE). Scanning electron microscopy (SEM) and Raman spectroscopy were utilized to characterize the working electrode surface. The electrochemical properties were studied using cyclic voltammetry (CV) and electrochemical impedance spectroscopy (EIS) with standard redox markers, and the results were compared with those obtained using a commercially available SPE and BDDE in a traditional configuration of an electrochemical cell. To validate the applicability of new sensors in electroanalysis, voltammetric methods were developed for the determination of selected biologically active substances, specifically the drugs mephenoxalone and atomoxetine, as well as the pesticide triticonazole. The next step involved the modification of the working electrode surface with gold nanoparticles through physical and electrochemical deposition. Modified sensors were characterized once again using SEM, Raman spectroscopy, CV, and EIS. The application possibilities of the modified sensors were tested in the analysis of the neurotransmitter dopamine.

Abstrakt
V rámci této disertační práce byly připraveny nové sítotiskové senzory (SPE) s chemicky deponovanou bórem dopovanou diamantovou elektrodou (BDDE). Pro charakterizaci povrchu pracovní elektrody těchto senzorů byla použita skenovací elektronová mikroskopie (SEM) a Ramanova spektroskopie. Jejich elektrochemické vlastnosti byly studovány s využitím cyklické voltametrie (CV) a elektrochemické impedanční spektroskopie (EIS) standardních redoxních markerů a dosažené výsledky byly porovnávány s komerčně dostupným SPE a BDDE v klasickém tříelektrodovém uspořádání elektrochemického článku. Pro ověření aplikovatelnosti nových senzorů v elektroanalýze byly vyvinuty voltametrické metody pro stanovení vybraných biologicky aktivních látek, konkrétně léčiv mefenoxalonu a atomoxetinu a pesticidu tritikonazolu. Dalším krokem byla modifikace povrchu pracovní elektrody zlatými nanočásticemi, a to fyzikální a elektrochemickou depozicí. Modifikované senzory byly charakterizovány pomocí SEM, Ramanovy spektroskopie, CV a EIS. Aplikační možnosti modifikovaných senzorů byly testovány při stanovení neurotransmiteru dopaminu.

Keywords
screen-printed sensor; boron-doped diamond electrode; modification; gold nanoparticles; electrochemical properties; electroanalysis

Klíčová slova
sítotiskový senzor; borem dopovaná diamantová elektroda; modifikace; zlaté nanočástice; elektrochemické vlastnosti; elektroanalýza

Table of Contents

Introduction

Electrochemical and voltammetric methods are gaining popularity each year, as evidenced by the increasing number of publications in the Web of Science. These methods offer advantages, including high sensitivity, rapid response, selectivity, miniaturization, portability, and cost-effectiveness, making them valuable for various applications. Professor Jaroslav Heyrovský, the founder of electrochemical methods, published his results as early as 1922 and later received the Nobel Prize for the discovery of polarography in 1959 [1]. The method involves measuring the current passing through a working electrode as a function of voltage [2]. Polarography and voltammetry differ in the choice of the working electrode. Polarography uses a dynamic dropping mercury electrode, while voltammetry utilizes stationary electrodes such as a hanging mercury drop electrode, metal or carbon electrodes [3–5]. Voltammetry can operate with two, three, or four-electrode set-up systems. The three-electrode system is the most common, consisting of a working, a reference, and an auxiliary electrode, allowing the measurement of the potential of the working electrode against the reference electrode in a no-current state. The most important element of voltammetric analysis is the material of the working electrode. Since the discovery of polarography, mercury has been the most commonly used electrode material, with its main advantages being a continuously renewing surface, ideal polarization of the entire drop, and a very wide usable potential window in the cathodic region. The disadvantage of mercury is its toxicity, which has led to a gradual reduction in the use of mercury electrodes, and despite their excellent electrochemical properties, they are essentially no longer used today.

The current research in electroanalytical chemistry is focused on new working electrodes and sensors that must meet criteria such as a wide potential range, stability, and low background current. Metal electrodes (gold, platinum, silver, palladium) are partially suitable, but they have limited selectivity and potential windows. Carbon electrodes, including glassy carbon, graphite electrodes, and carbon nanomaterials, are another option, with their properties varying according to the nature of the carbon. An exceptional electrode material showing excellent electrochemical properties is boron-doped diamond [6]. To achieve better selectivity and reduce the detection limit, electrode surfaces are often modified with metal nanoparticles, polymers, and biomolecules [7]. In addition to new electrode materials, the miniaturization of electrochemical cells is also important and offers numerous advantages. It conserves resources, reduces costs, and promotes more environmentally friendly approach in analytical chemistry. Miniaturization shortens the analysis time due to smaller volumes of reagents, enabling faster reaction kinetics. These systems are easily portable, which is advantageous for medical applications and environmental monitoring, allowing real-time data collection for quick decision-making.

The presented dissertation is focused on the issue of new electrochemical screen-printed sensors with a chemically deposited boron-doped diamond electrode (BDDE), their characterization and application in the analysis of selected biologically active substances. The objectives of this dissertation thesis were defined as follows:

1. Literary research on the topic of working electrodes in voltammetry with a focus on BDDE and especially on the possibilities of its modification.
2. Study and description of the electrochemical behavior of selected biologically active substances (pesticides and drugs) and development of voltammetric

methods for teir determination using BDDE in a classic three-electrode arrangement of an electrochemical cell.

3. Characterization of new laboratory-made screen-printed sensors with BDDE as a working electrode – surface and electrochemical properties.
4. Application of new printed sensors with BDDE in the analysis of substances for which determination methods have been developed under point 2.
5. Surface modification of BDDE on screen-printed sensors with gold nanoparticles, characterization and application of modified sensors in electroanalysis.

1. Theoretical part

1.1 Boron-doped diamond electrode

In the early 1990s, boron-doped diamond electrodes (BDDE) were introduced in the field of electroanalytical chemistry [8–10]. BDDE offers several advantages, including chemical and electrochemical stability, wide potential window, high electrical conductivity, low background current, and biocompatibility [8–10]. While pure diamond is an insulator, it can be doped with atoms, typically boron, for electrochemical applications. The concentration of dopants significantly influences the electrochemical properties of BDDE, with boron being preferred due to its low charge carrier activation energy of 0.37 eV [11].

To prepare diamond films, chemical vapor deposition (CVD) is employed, using a mixture of methane and hydrogen with diborane as the boron source [12]. Substrates are commonly made from silicon, molybdenum, or tungsten. The B/C ratio, measured in ppm, denotes the ratio of boron atoms to carbon atoms during diamond film formation, and it influences both the volume and the surface concentration of boron. Doping diamond with boron allows for a range of conductivity from semiconductor to metallic [13]. The B/C ratio affects a morphology, a quality, and an electrochemical properties of BDDE [14]. Studies employing techniques such as Raman spectroscopy, scanning electron and atomic force microscopy's, electrochemical impedance spectroscopy, cyclic voltammetry, and others have shown that BDDE with B/C ratios between 500-1000 ppm exhibit semiconductor conductivity, while those with B/C ratios of 2000 or higher display metallic conductivity [13,14]. An increase in the B/C ratio narrows the usable potential range, generally leading to improved electrochemical properties of the electrodes. The electrode preparation process is crucial and involves anodic or cathodic polarization, cyclic voltammetry, and polishing [6]. A supplemental pretreatment step includes the chemical attachment of amino or carboxyl groups, allowing the immobilization of biomolecules such as DNA or enzymes [15]. The modification of BDDE with various materials, including metal nanoparticles, organic molecules, biomolecules, and carbon materials, enhances their electrochemical properties and broadens their applications in sensing and analytical chemistry [16].

BDDE has found extensive applications in electroanalytical chemistry and can sometimes replace mercury electrodes, contributing to environmental protection. These electrodes are employed for the determination of various substances, including drugs, pesticides, biomarkers, and environmental contaminants, showing promise in wastewater treatment [6,17–26].

1.2 Screen-printed electrodes

Currently, one of the significant trends in analytical and electroanalytical chemistry is the miniaturization of analytical systems. These needs are well served by screen-printed electrodes (SPE) produced using various inks on polyvinyl chloride or ceramic substrates. They offer advantages such as low costs, customized design, easy mass production, and can be used as disposable sensors [27–31]. SPEs can be tailored to detect a wide range of analytes, including gases, liquids, and biomolecules, making them suitable for on-site diagnostics, environmental monitoring, food safety, and other applications requiring fast, cost-effective, and portable sensing devices [32]. A variety

of applications of SPE in different areas of analysis have been described in the literature. As mentioned earlier, choosing an appropriate sensor, especially the working electrode, is crucial for successful application. Sensors with BDDE are promising due to their exceptional properties, including high sensitivity, reproducibility, and stability. These diamond electrodes can be applied to SPE using inkjet printing of inks containing BDD powder or using CVD [33,34]. Commercially available SPE with BDDE have been used, particularly in drug analysis [32,34–36]. However, these sensors are no longer available, as production has ceased.

In this Ph.D. thesis, new lab-made screen-printed sensors with BDDE (LM-SP/BDDE) manufactured at the Slovak University of Technology in Bratislava by group of M. Vojs are introduced. The preparation, characterization, testing, and application of these new sensors have been described in the author's attached publications. Over the past two years, the use of these sensors has expanded to other research institutions.

1.3 Studied substances

1.3.1. Mephenoxalone

Mephenoxalone (MNL, 5-[(2-methoxyphenoxy)methyl]-1,3-oxazolidin-2-one, Figure 1A) is a muscle relaxant used to alleviate muscle spasms and pain while also providing anxiety relief in individuals [37–39]. It acts by central nervous system depression, leading to reduced muscle tone and skeletal muscle relaxation [40–43]. It possesses muscle relaxant properties and offers significant sedation without causing severe side effects[42,44]. When combined with paracetamol, it exhibits analgesic characteristics [45]. It is typically used in conjunction with physical therapy and other treatments to manage musculoskeletal disorders like back pain, neck pain, and muscle tension. While generally well-tolerated by most patients, it may cause dizziness, drowsiness, and other side effects in some individuals. Studies on dogs and rats have shown that prolonged exposure to MNL results in anemia, weight loss, hemolytic anemia, and death [37,38,46,47]. The widespread use of this medication, along with potential side effects, necessitates clear and precise monitoring of MNL concentration levels in pharmaceutical products, biological samples, and the environment. To date, there is no information available regarding the electrochemical behavior of MNL, and literature lacks information on the possibility of its voltammetric determination.

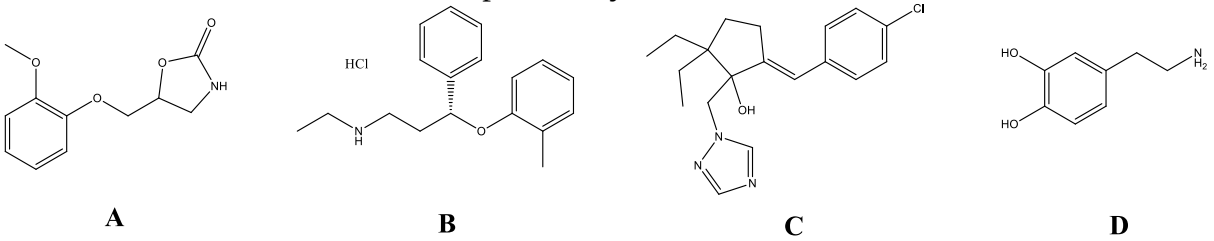

Figure 1 *Structural formula of MNL (A), ATX (B), TTC (C), DA (D)*

1.3.2. Atomoxetine

Atomoxetine (ATX, (R)-N-methyl-3-phenyl-3-(o-tolyloxy)propan-1-amine, Figure 1B), is a medication used to treat attention-deficit/hyperactivity disorder symptoms (ADHD) [48]. It acts as a central sympathomimetic by selectively inhibiting

norepinephrine reuptake and blocking the presynaptic norepinephrine transporter [49,50]. One of ATX's advantages is its non-addictive nature, but it can lead to side effects such as digestive problems, loss of appetite, headaches, dry mouth, behavioral changes, sleep disturbances, and allergic reactions [51]. In the available literature, only one study addresses the electrochemical behavior of ATX and method development for its determination [52]. Using a glassy carbon electrode, researchers found that ATX exhibits a distinct oxidation peak at around +1.5 V in 0.1 mol L^{-1} $HClO_4$ [53]. Differential pulse voltammetry yielded a linear dynamic range from 0.1 to 1.0 mmol L^{-1} and a calculated limit of detection (LOD) of 69 μmol L^{-1}. This method was successfully applied for drug sample analysis [52].

1.3.3. Triticonazole

Triticonazole (TTC, rac-(5E)-5-(4-chlorobenzylidene)-2,2-dimethyl-1-(1H-1,2,4-triazol-1-ylmethyl)cyclopentanol, Figure 1C) is a systemic fungicide used in agriculture to protect crops from various fungal diseases [54,55]. It belongs to the group of triazole fungicides that inhibit the biosynthesis of ergosterol, an essential component of fungal cell membranes [56]. TTC is effective against a broad spectrum of fungal pathogens, including *Ascomycetes*, *Basidiomycetes*, and *Deuteromycetes*. It is commonly used to safeguard crops such as cereals, oilseeds, fruits, and vegetables, available in various forms, including liquids, emusifiable concentrates, and granules [57–59]. Although the patent use of triazole fungicides, including TTC, emerged in 2005, its extensive use makes it a potential environmental hazard [59]. At high concentrations, TTC can act as an endocrine disruptor, substances that interfere with the synthesis, secretion, transport, binding, action, or elimination of natural hormones in the body, negatively impacting development, behavior, fertility, and homeostasis [60,61]. The risk is associated with cumulative exposure to triazole fungicides, their metabolites, or complexes with metal ions (*e.g.*, Zn or Cu), altering their behavior in the environment and biological activity [62,63]. Voltammetric determination of TTC has not yet been described in the literature.

1.3.4. Dopamine

Dopamine (DA, 4-(2-aminoethyl)benzen-1,2-diol, Figure 1D) is a neurotransmitter involved in a wide range of physiological and behavioral processes, including movement, motivation, reward, and reinforcement of behavior [64,65]. It is a chemical messenger that transmits signals between nerve cells in the brain and plays a key role in regulating mood, attention, and cognition [66]. DA is produced in the brain by a group of cells known as dopaminergic neurons, which are found in various brain regions, including the substantia nigra and the ventral tegmental area. The release of DA in response to specific stimuli, such as food, sex, or drug abuse, triggers feelings of pleasure and reinforces behavior. DA also contributes to the regulation of movement, and its deficiency in the brain is associated with Parkinson's disease, a progressive neurological disorder characterized by tremors, stiffness, and movement difficulties [67,68]. Excessive dopamine activity is also involved in certain psychiatric disorders, such as schizophrenia, which is marked by delusions, hallucinations, and disrupted thinking [67,68]. The electrochemical oxidation of DA on the electrode surface results in the formation of various oxidation products, including dopamine-o-quinone, 5,6-dihydroxyindole, and aminochrome [69].

2. Experimental part

2.1 Chemicals

Stock solutions of 0.001 mol L^{-1} MNL (purity > 99%, Sigma-Aldrich), TTC (purity > 99%, Sigma-Aldrich), ATX (purity > 99%, Sigma-Aldrich), and DA (purity > 99%, Sigma-Aldrich) were prepared by dissolving the powder in acetonitrile (Ing. Petr Švec – PENTA s.r.o., Czech Republic) and stored in a refrigerator (+4.0 °C) without access to light. Lower concentration solutions were prepared fresh each day by diluting with the supporting electrolyte. Britton-Robinson buffer (BRB) was composed of a mixture of acidic and alkaline components. The acidic component was formed by a solution of H_3PO_4 (0.04 mol L^{-1}), H_3BO_3 (0.04 mol L^{-1}), and CH_3COOH (0.04 mol L^{-1}), when the solution was prepared by diluting concentrated acids (85% H_3PO_4, 99% CH_3COOH, Ing. Petr Švec - PENTA s.r.o., Czech Republic) and by dissolving the weighted amount of H_3BO_3 (Sigma-Aldrich). The alkaline component was a NaOH solution with a concentration of 0.2 mol L^{-1} (Ing. Petr Švec – PENTA s.r.o., Czech Republic). Solutions of HNO_3 (0.1 mol L^{-1}), H_2SO_4 (0.1 and 0.05 mol L^{-1}), HCl (0.1 mol L^{-1}), and $HClO_4$ (0.1 mol L^{-1}) were prepared by diluting concentrated acids (65% HNO_3, 96% H_2SO4, 35% HCl, and 64.5% $HClO_4$ (all from Ing. Petr Švec – PENTA s.r.o., Czech Republic). A stock solution of 0.1 mol L^{-1} KCl was prepared by dissolving an appropriate amount of powder (Ing. Petr Švec – PENTA s.r.o., Czech Republic) in distilled water. Standard solutions of 0.625 and 2.5 mmol L^{-1} $K_3[Fe(CN)_6]$ and $[Ru(NH_3)_6]Cl_3$ (both > 99% purity, Sigma-Aldrich) were prepared by dissolving in 0.1 mol L^{-1} KCl. A solution of $HAuCl_4 \cdot 4H_2O$ (Sigma-Aldrich) with a concentration of 1 mmol L^{-1} in 0.1 mol L^{-1} H_2SO_4 was used for the electrodeposition of AuNPs. A KCN (Sigma-Aldrich) solution (0.1 mol L^{-1}) was used to remove AuNPs.

The various pharmaceutical and pesticide preparations were analyzed. Specifically, the pharmaceutical preparations were Dimexol 200 mg (Glenmark Pharmaceuticals Distribution s.r.o., Czech Republic) containing the active substance MNL (manufacturer-declared content of 200 mg), and Strattera 60MG (Eli Lilly, Czech Republic) containing the active substance ATX (60 mg). Human I biocomplex serum (from Biosystems S.A., Spain) was used as the matrix for analyzing the biological sample. Additionally, a commercially available pesticide preparation Saprol (Substral, France) containing the active substance TTC (10 g) and sold in emulsion form was analyzed as well.

2.2 Instrumentation

Voltammetric measurements were performed using an Autolab PGSTAT204 analyzer with an electrochemical impedance spectroscopy (EIS) module FRA32M (Metrohm Autolab, The Netherlands) equipped with Nova 2.1.5 software. In the case of a conventional three-electrode electrochemical cell arrangement, BDDE (BioLogic, France, surface area 7.07 mm^2, inner diameter 3.0 mm, resistivity 0.075 Ω cm with B/C ratio at 1000 ppm deposition) was used as a working electrode (WE), saturated silver chloride electrode (Ag/AgCl/KCl(sat.)) as a reference (RE) and platinum wire as an auxiliary electrode (CE) (both Monokrystaly, Czech Republic). In addition, the

following two types of SPE with BDDE were used: (i) commercially available SPE (SP/BDDE, Metrohm/DropSens, Czech Republic) with BDD WE (area 10.17 mm^2, inner diameter 3.6 mm, B/C was not specified by the manufacturer), carbon CE and silver RE and (ii) laboratory-prepared SPE (LM-SP/BDDE) formed from BDD as both WE and CE and Ag/AgCl pseudo-RE. 3 types of LM-SP/BDDE were tested with different working electrode area (0.785; 3.14 and 7.07 mm^2, inner diameter 1.0, 2.0 and 3.0 mm, B/C 312,500 in gas phase during deposition, resistivity 0.017 Ω cm). All tested sensors are shown in Figure 2. 3LM-SP/BDDEs were used for modification with gold nanoparticles (AuNPs). Vacuum evaporation was used to modify SPE with AuNPs of different sizes (nAu-SP/BDDE, where n = 5.0, 15 and 50 nm refers to the thickness of the gold layer deposited by physical evaporation) and with nanoporous gold nanoparticles (pAu-SP/BDDE). For comparison, SP/BDDE modified with gold nanoparticles by electrochemical deposition (eAu-SP/BDDE) and SP/BDDE, in which the WE was completely covered with a gold layer (Au-SP/BDDE), were also used.

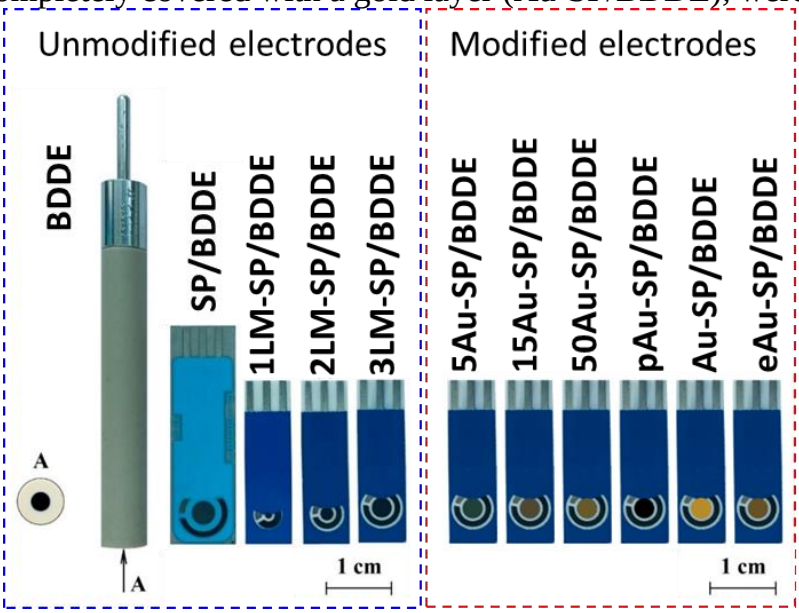

Figure 2 *Applied sensors*

Scanning electron microscopy (JEOL 7500f, viewing angle 45°, from JEOL Ltd., Tokyo, JP) was used to examine the morphology of the surface and the thickness of the BDD film. Analysis of AuNPs' size was conducted using ImageJ software (from the National Institutes of Health and Laboratory for Optical and Computational Instrumentation, University of Wisconsin). The size distribution of NPs (at least 50 particles) on the electrode surface was analyzed using Gaussian function in OriginPro 9.0 software (OriginLab Corporation, Northampton, USA). The chemical structure of deposited films was assessed by Raman spectroscopy (633 nm Dilor system, 5 μm spot diameter, Spectroscopy&Imaging, Germany). The Agilent 1260 Infinity II Prime LC System liquid chromatograph (Agilent, United States) with a DAD detector was used for HPLC comparative analysis of model solutions and real samples. For the analysis of MNL oxidation products, an Agilent 7890A gas chromatograph with a mass selective detector (MSD) Agilent 5975C (Agilent, Santa Clara, CA, USA) was used. Solutions were prepared using the Accumet AB150 pH meter (Fisher Scientific, Czech Republic) and the Bandelin Sonorex ultrasonic bath (Schalltec GmbH, Germany).

Spectroelectrochemical absorption spectra were obtained using the Nicolet iS50 FTIR spectrometer in the wavenumber range of 4000-650 cm^{-1}.

2.3 Preparation of screen-printed sensors

The SPE was produced during an internship guided by Dr. Marian Vojs` research group at the Slovak Technical University in Bratislava (Slovak Diamond Group). The preparation steps for the LM-SP/BDDE are detailed in Figure 3A. BDD deposition was performed via microwave plasma chemical vapor deposition (MWCVD) in a linear antenna reactor, utilizing 6.0 kW of microwave power with specific timing and phase changes. The deposition process lasted 30 hours at a substrate temperature of 590 °C and a pressure of 30 Pa. The concentration of trimethyl borate as a boron source was 1.0%, and CO_2 concentration was 0.2% relative to background hydrogen, resulting in a B/C ratio of 312,500 ppm in the gas mixture. The silver electrode and insulating layer were screen-printed using a photochemical template prepared with FOTECOAT 1019 BLUE photosensitive emulsion. The printing process employed a semi-automatic machine with SERILOR HR1 P0 85°Sh polyurethane screed, AST6025 silver printing paste, and a polyester mesh. For the reference electrode (RE), two layers were printed using the "wet-on-wet" method. The Ag/AgCl transformation was achieved through electrochemical chlorination, applying +0.7 V potential for 30 seconds in 0.1 mol L^{-1} KCl solution with RE acting as the working electrode while being continuously stirred.

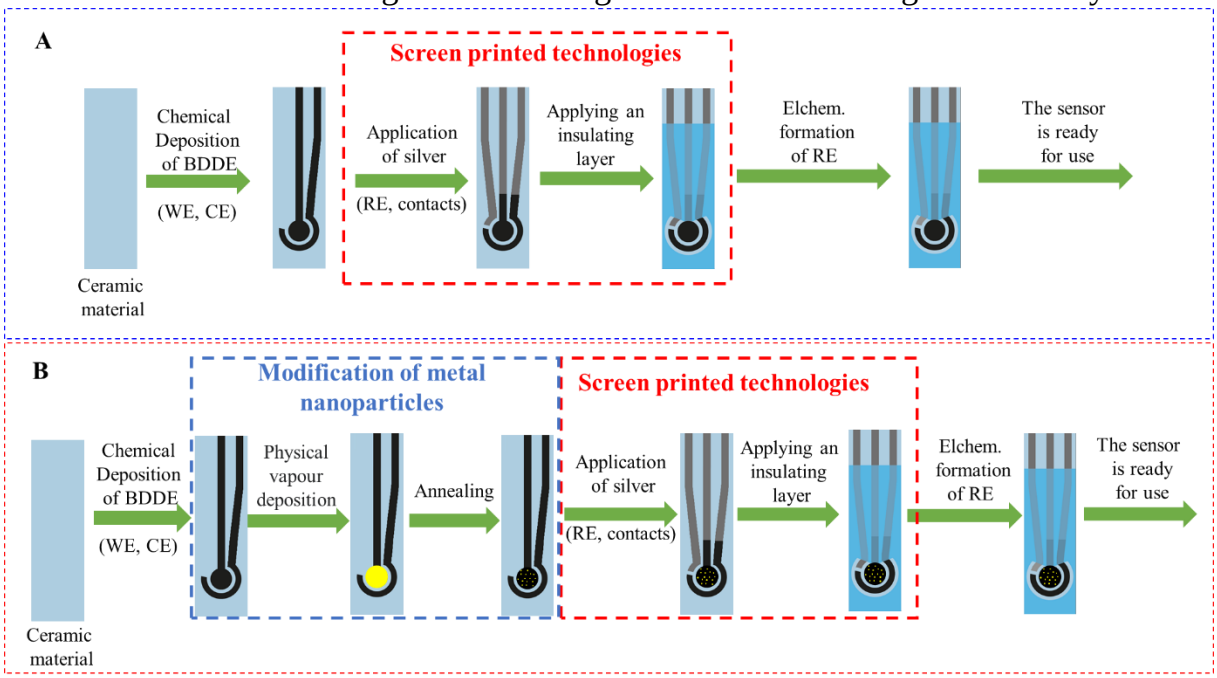

Figure 3 *Preparation of LM-SP/BDDE (A) and LM-SP/BDDE modified with gold nanoparticles (B)*

The modification of BDDE with AuNPs and porous gold nanoparticles (pAuNPs) was performed during the fabrication of the printed sensor, specifically after the deposition of the BDD layer by MWCVD method (Figure 3B). Sensors designated as nAu-SP/BDDE were modified with AuNPs by physical deposition (PD). Au layers of different thicknesses (n = 5.0, 15, and 50 nm) were formed on the BDD surface by

thermal evaporation of Au in high vacuum. Subsequent annealing in a nitrogen atmosphere at a temperature of 600°C resulted in the final form of nAuNPs with an ensured homogeneous dispersion. The NP size varied depending on the thickness of the Au film. Finally, porous pAuNPs were prepared by evaporation of the Au/Ag bilayer, annealing to form the Au/Ag alloy (N^2, 600°C) and wet etching in hydrofluoric acid to remove Ag [70].

Electrochemical modification of the surface of the working electrode with AuNPs was performed after the completion of the production of LM-SP/BDDE in an environment containing 1.0 mmol L^{-1} $HAuCl_4 \cdot 4H_2O$ in a solution of 0.1 mol L^{-1} H_2SO_4. This electrolyte composition was chosen based on information available in the literature [71–74]. The potential (E_{dep}) and time (t_{dep}) of electrochemical deposition (ED) were optimized, when 0 V and 50 s were used as the optimal parameters for the modification.

2.4 Procedures

The activation procedure for BDDE before measurements was optimized for each studied analyte. It was found that the same approach could be used for all cases. Before starting, BDDE was activated by running 20 cyclic voltammograms in a potential range from –1.5 V to +2.2 V, at a scan rate (v) of 100 mV s^{-1}. It was observed that there was no need to reactivate or regenerate the electrode between measurements. SP/BDDE sensors were also activated using CV, with the same parameters, but only 10 cycles for response stabilization. For modified SP/BDDE, no activation procedure was used to prevent the dissolution of AuNPs.

Cyclic voltammetry (CV) was used to investigate the electrochemical behavior of MNL, ATX, TTC, and DA, as well as the influence of pH of the supporting electrolyte and the scan rate. In the absence of specific instructions, measurements were taken within a potential range from –1.5 V to +2.2 V with v = 100 mV s^{-1}. When exploring the impact of scan rate, v varied from 25 to 500 mV s^{-1}. Given their impressive sensitivity, square-wave voltammetry (SWV) and differential pulse voltammetry (DPV) were employed for detecting the substances. Initially, a suitable supporting electrolyte was selected, experimenting with different inorganic acids, BRB (pH 2-12), or NaOH solution. Afterward, the voltammetric methods` parameters were fine-tuned. For DPV, this meant adjusting v, which ranged from 10 to 100 mV s^{-1}, the pulse amplitude (A) between 10 and 100 mV, and the modulation time (t_m) from 10 to 100 ms. In the case of SWV the followed parameters were optimized, v (10-100 mV s^{-1}), amplitude (10-100 mV), and frequency (f = 5-50 Hz). Finally, tested how electrode surface pre-treatment influenced peak height, shape, and repeatability using these procedures: (i) cathodic polarization (E = –1.0 V, t = 300 s), (ii) anodic polarization (E = +2.2 V, t = 300 s), (iii) cycling (20 CV cycles, E_{in} = –1.0 V, E_{switch} = +2.2 V, E_{fin} = +2.2 V, v = 100 mV s^{-1}), and (iv) manual polishing on aluminum (t = 60 s). After each procedure, measured 11 voltammograms of the analyte at a specific concentration, assessed peak height, and calculated the corresponding relative standard deviation (RSD).

For the model solutions analyses, the samples were prepared by diluting the stock solution of the analytes with a supporting electrolyte to achieve the desired concentration. A suitable volume of this solution was then added into an electrochemical

cell. The analysis followed the standard addition method and was repeated five times. From the obtained results, essential statistical parameters, such as the average concentration with the corresponding confidence interval, recovery, and RSD, were calculated. Samples of pharmaceutical products were prepared for analysis by dissolving tablets of Dimexol (MNL) or contents of capsules of Strattery (ATX) in an appropriate volume of acetonitrile while applying ultrasound. The sample of the pesticide emulsion product, Substral (TTC), was also dissolved in acetonitrile. Subsequently, a suitable volume of the sample solution was transferred to the electrochemical cell containing the supporting electrolyte, and the analysis was performed using the standard addition method, with the above-mentioned statistical parameters calculated. Serum analysis for MNL determination was conducted using SPE, enabling analysis in small sample volumes. The analysis was carried out in a droplet of serum with a volume of 50 μL. Additionally, there was no need to add a supporting electrolyte to the serum sample, as the serum had sufficient ionic strength, ensuring ample conductivity of the medium. The analysis employed the calibration curve method, where a calibration series was prepared by adding an appropriate volume of diluted standard MNL solution to the serum.

CV was employed for the electrochemical characterization of the tested sensors using selected redox markers. The first used *"outer-sphere"* redox system was $[Ru(NH_3)_6]^{2+/3+}$ [13,75–77]. *"Inner-sphere"* redox markers included $[Fe(CN)_6]^{4-/3-}$ and DA [9,13,75,76,78,79]. Initially, ten CV cycles were measured using all tested sensors for all mentioned substances to evaluate measurement repeatability. Subsequently, scan rate dependencies were measured to determine or confirm the controlling steps of the observed electrochemical reactions.

Experiments using EIS were conducted in the frequency range from 10 kHz to 1.0 Hz with a pulse amplitude of 10 mV. For the characterization of unmodified SP/BDDE, complexes $[Fe(CN)_6]^{4-/3-}$ and $[Ru(NH_3)_6]^{2+/3+}$ served as markers, and for sensors modified with AuNPs, DA was also included. To determine the half-wave potentials ($\Delta E_{1/2}$), cyclic voltammograms of $[Fe(CN)_6]^{4-/3-}$, $[Ru(NH_3)_6]^{2+/3+}$, and DA in KCl were measured first. $\Delta E_{1/2}$ values were calculated for each sensor type as half the difference between the oxidation and reduction peak potentials. These values were then used as initial potentials in EIS for each specific sensor type. In the case of SP/BDDE, five electrodes of each type were used, and three repeated measurements were performed on each. The values of individual elements in electrical equivalent circuits (EECs) (R([R]/Q) for the $[Fe(CN)_6]^{4-/3-}$ complex, R([RW]/Q) for the $[Ru(NH_3)_6]^{2+/3+}$ complex) were calculated using FRA simulation in NOVA 2.1.5 software. In the case of characterization of electrodes modified with AuNPs, the following equivalent schemes were used: for $[Fe(CN)_6]^{4-/3-}$ and DA – R([RW]/Q for $[Ru(NH_3)_6]^{2+/3+}$ – [RW].

The parameters of calibration curves with their corresponding confidence intervals at a significance level of $\alpha = 0.05$ were calculated using OriginPro 9. The limit of detection (LOD) was calculated as a threefold of the standard deviation and the limit of quantification (LOQ) as a tenfold of the standard deviation of the intercept divided by the slope of the respective linear concentration dependency [80]. To ensure comparability of results achieved using working electrodes with different surface areas, the current values were converted to current density (j). The heterogeneous rate constant of electron transfer (k^0_{app}) was calculated using the Nicholson equation [81]. The reversibility of the electrode reaction was calculated as a mathematical function [81].

3. Results and discussion

3.1 Voltammetric determination of studied compounds

The electrochemical behavior of MNL, TTC, ATX, and DA was investigated using CV on BDDE in traditional configuration of electrochemical cell. It was found that all these biologically active compounds exhibited electrochemical activity and had a current response suitable for analytical detection. Due to the height sensitivity, the SWV and DPV methods were employed for the development of a voltammetric determination method, the optimized parameters are provided in the experimental part. After optimizing the parameters of the voltammetric methods, concentration dependences were measured, and examples of the obtained voltammograms are shown in Figure 4. Statistical parameters describing these dependences were calculated and are presented in Table 1. Subsequently, an analysis of model solutions and real pharmaceutical preparations (Dimexol (MNL) and Strattera (ATX)) as well as pesticide preparation (Substral (TTC)) was successfully performed. The accuracy and repeatability of measurements were verified through the calculation of RSD. For MNL and TTC, the developed method was compared with the standard method of HPLC-DAD, and the relevance of these measurements was demonstrated using a *t*-test [82]. Additionally, mechanism of the electrochemical oxidation of MNL was proposed. It was confirmed through the identification of the products of preparative electrolysis using GC-MS and applying spectroelectrochemical measurements.

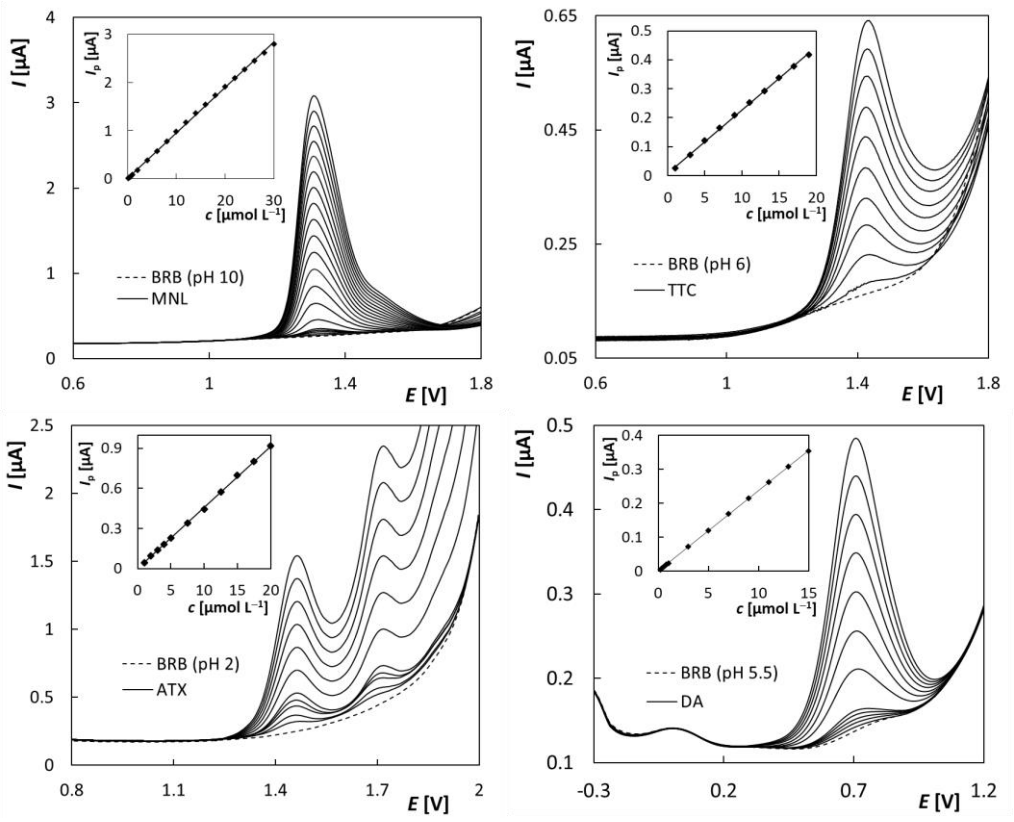

Figure 4 *SW (MNL, TTC, DA) and DP (ATX) voltammograms in dependence on the concentration measured using BDDE with the appropriate linear dependences of* I_p *on c*

Table 1 *Summary of statistical parameters for the determination of MNL, TTC, ATX, DA*

	MNL	TTC	ATX	DA
Method	SWV	SWV	DPV	SWV
pH of BRB	10	6	2	5.5
LDR [μmol L^{-1}]	0.1-30	1-20	0.2-20	0.2-286
Slope [nA μmol L^{-1}]	(94.67±0.37)	(21.69±0.15)	(45.78±0.19)	(25.53±0.13)
Intercept [nA]	(6.91±5.72)	(10.34±1.84)	(0.66±0.59)	(7.41±1.20)
r	0.9997	0.9996	0.9999	0.9998
LOD [nmol L^{-1}]	55	250	39	62
LOQ [nmol L^{-1}]	180	850	130	207
RSD_{11} [%]	0.9	2.5	5.0	1.4
Sample	pharmaceutical preparation	pesticide preparation	pharmaceutical preparation	urine
RSD_5 [%]	1.8	5.9	2.8	3.0

3.2 New screen-printed sensors with BDDE

3.2.1 Surface characterization

In the context of this Ph.D. thesis, a LM-SP/BDDE were prepared, and their surface and electrochemical properties were thoroughly investigated. Furthermore, their potential applications in the analysis of selected electroactive substances were explored.

An SEM image (Figure 5A) illustrates a thin BDD film that fabricated on Al_2O_3 substrate. The grain size of this film varies within the range of 0.2 to 1.0 μm. After 30 hours of growth, the film thickness measures approximately 3.5 μm, ensuring an uniformly covered ceramic substrate. Raman spectra, obtained using excitation wavelengths of 325 nm and 633 nm (Figure 5B), display characteristic peaks associated with heavily BDD. Specifically, the B_1 (480 cm^{-1}) and B_2 (1220 cm^{-1}) bands are attributed to the incorporation of boron into the diamond's structure. The peak observed at the zero phonon line (ZCP_D) corresponds to diamond, while the bands at 1360 cm^{-1} and 1570 cm^{-1} correspond to amorphous carbon and sp^2-bonded carbon [83,84].

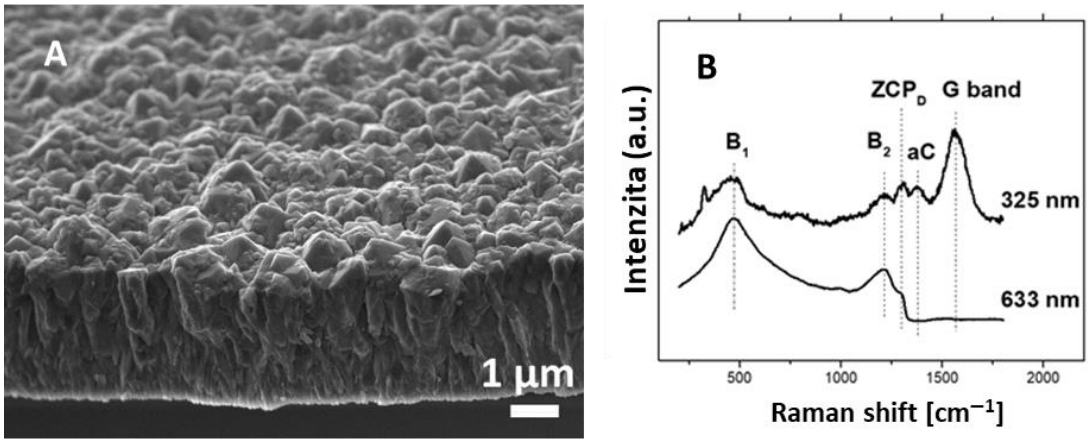

Figure 5 *SEM image of the BDD film on an Al_2O_3 substrate (at a 45° viewing angle) (A), and the Raman spectra of the BDD film obtained with excitations at 325 nm and 633 nm (B)*

3.2.2 Electrochemical properties

The electrochemical properties of LM-SP/BDDE were examined using CV, and the results were compared with those obtained using BDDE in a classical three-electrode set-up and a commercially available SP/BDDE. The first tested parameter was the usable potential range or electrochemical windows of each sensor in the supporting electrolyte of 0.1 mol L^{-1} H_2SO_4. The anodic and cathodic potential limits were defined as the potential at which the value of j exceeded ±2.0 μA mm^{-2}. All tested electrodes provided similarly wide potential windows, more than 3.0 V. The widest potential range was observed for BDDE, which corresponds to a lower level of boron doping [13,14].

The reversibility of electrode reactions was investigated. Figure 4A shows cyclic voltammograms for $[Fe(CN)_6]^{4-/3-}$ on all tested electrodes, revealing relatively similar j_p values. The highest oxidation and reduction peaks were observed on 2LM- and 3LM-SP/BDDE. The j_{pa}/j_{pc} parameter for all sensors confirmed the reversibility of the electrode reaction, remaining close to 1.0. ΔE_p exceeded the theoretical value of 59 mV, likely due to the *"inner-sphere*" nature of this marker, influenced by the electrode surface quality. Notably, SP/BDDE exhibited the least favorable result (ΔE_p = 395 mV), while LM-SP/BDDE demonstrated increased reversibility as the working electrode area expanded (ΔE_p = 115 mV for 3LM-SP/BDDE). Moving to Figure 6B, depicting cyclic voltammograms for the $[Ru(NH_3)_6]^{2+/3+}$ complex, the j_{pa}/j_{pc} parameter indicated a reversible reaction (ranging from 0.96 to 1.03). Unlike $[Fe(CN)_6]^{4-/3-}$, ΔE_p values for $[Ru(NH_3)_6]^{2+/3+}$ closely approached the theoretical value of 59 mV, indicating a one-electron reversible electrode reaction due to the *"outer-sphere*" nature of the redox system [85]. Exceptional reversibility was confirmed, particularly for LM-SP/BDDE and classical BDDE (ΔE_p = 59-65 mV), with a larger discrepancy observed for SP/BDDE (ΔE_p = 85 mV). Finally, it's important to note the considerable potential change in redox signals between SPEs and BDDE in the traditional three-electrode setup. This alteration arises due to the utilization of pseudo-reference electrodes with SPEs.

The effect of scan rate (from 25 to 500 mV s^{-1}) on voltammetric responses for both redox markers was investigated. As the v increased, responses also grew, with non-linear j_p *vs.* v dependence. However, $j_p = f(v^{1/2})$ plots displayed linear trends, typical of diffusion-controlled electrode reactions common with BDDE due to low analyte adsorption. The slopes indicated diffusion's dominance as the controlling process. The slope of logarithmic dependence $log\ (j_p) = f(log\ (v))$ was close to theoretical value of 0.5, particularly for the $[Ru(NH_3)_6]^{2+/3+}$ complex. Apparent rate constants (k^0_{app}) were not corrected for double-layer effects [81]. A k^0_{app} values for $[Fe(CN)_6]^{4-/3-}$ spanned three orders of magnitude (2.10×10^{-3} to 5.70×10^{-5} cm s^{-1}), confirming marker sensitivity to surface characteristics. LM-SP/BDDEs and BDDE exhibited high k^0_{app} values, especially 3LM-SP/BDDE. SP/BDDE had a significantly lower k^0_{app}. $[Ru(NH_3)_6]^{2+/3+}$ k^0_{app} values were consistent, ranging narrowly from 4.40×10^{-3} to 3.16×10^{-3} cm s^{-1}. These align with the *"outer-sphere"* marker characteristics, as per published results [13,14,84]. Superior electrochemical properties were evident with 2LM- and 3LM-SP/BDDE.

The acquired EIS spectra (Figure 6E, F) show a correlation with the CV results, where electrodes with the lowest electron transfer resistance R_{ct} values exhibit the sharpest peaks and best reversibility. For $[Fe(CN)_6]^{4-/3-}$ (Figure 6E), SP/BDDE displayed the highest R_{ct} value of 40.1 kΩ, indicating the largest ΔE_p between oxidation and reduction peaks. In contrast, LM-SP/BDDE showed decreasing R_{ct} values as the WE surface area increased, with values of 21.6, 7.7, and 2.4 kΩ for electrode diameters of 1.0, 2.0, and 3.0 mm, respectively. However, when normalized by the electrode surface area, the values were quite similar (0.17, 0.24, and 0.17 kΩ cm^2). BDDE and SP/BDDE exhibited R_{ct} values of 11.7 kΩ and 0.83 kΩ cm^2, and 40.1 kΩ and 4.1 kΩ cm^2, respectively. For $[Ru(NH_3)_6]^{2+/3+}$ (Figure 6F), BDDE and SP/BDDE displayed significantly lower R_{ct} values of 1.0 kΩ (71.8 Ω cm^2) and 0.12 kΩ (12.3 Ω cm^2), respectively. LM-SP/BDDE showed R_{ct} values of 1.19, 0.94, and 1.98 Ω cm^2 for electrodes with diameters of 1.0, 2.0, and 3.0 mm. Higher variability in values was observed for 2LM-SP/BDDE and 3LM-SP/BDDE, with low R_{ct} values around 30 Ω due to challenging EEC simulation and fitting. These lower R_{ct} values on highly BDDE align with their electrochemical behavior [13,14]. The consistent low R_{ct} values on the tested electrodes confirm the long-term stability of H-termination, in contrast to O-terminated BDDE, which shows significantly higher R_{ct} values, as reported by Oliveira and Oliveira-Brett [86].

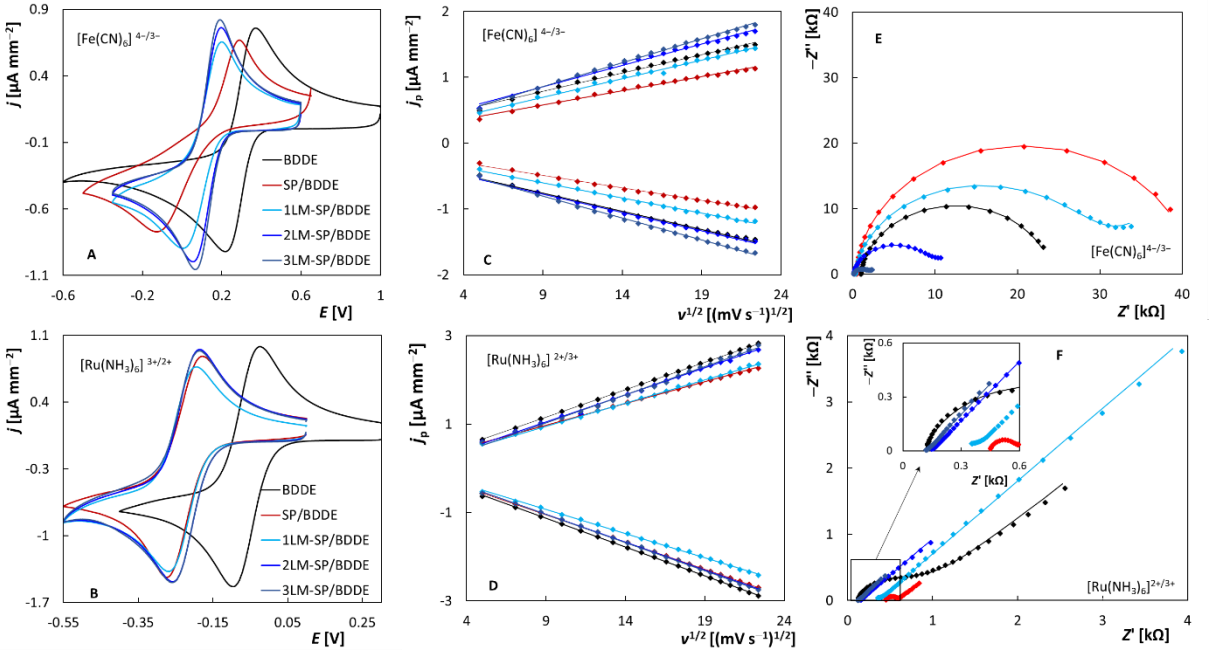

Figure 6 *Cyclic voltammograms of $[Fe(CN)_6]^{4-/3-}$ (A) and $Ru(NH_3)_6]^{2+/3+}$ (B), dependences $j_p = f(v^{1/2})$ (C, D), and electrochemical impedance spectra (E, F) recorded on the tested sensors.*

3.2.3 Application in electroanalysis

One of the objectives of this Ph.D. thesis was to explore the application potential of the new LM-SP/BDDE. For this purpose, the drugs MNL and ATX, along with the fungicide TTC, were chosen as analytes. Methods developed for these analytes using BDDE were adopted for tested SPEs.

The electrochemical behavior of MNL and TTC was investigated using all tested sensors, while for ATX, the results from BDDE, SP/BDDE, and 2LM-SP/BDDE were compared. Figure 7 displays the cyclic voltammograms of MNL (A), TTC (B), and ATX (C). While only one oxidation peak of MNL was observed on BDDE, the printed sensors exhibited additional poorly defined signals (Figure 7A). The obtained j_p values for MNL peak were comparable for all sensors. In the case of TTC (Figure 7B), in addition to the same anodic response as observed on BDDE, another less developed and poorly evaluable peak in the more positive potential region was observed on the SPE sensors. Its shape was significantly affected by the degradation of the supporting electrolyte. Figure 7C for ATX reveals that the voltammetric curves obtained on all tested sensors are more complex and contain multiple anodic signals compared to BDDE. For analytical purposes, the first oxidation signals observed on each SPE, corresponding to the response on BDDE, appeared suitable for all analytes.

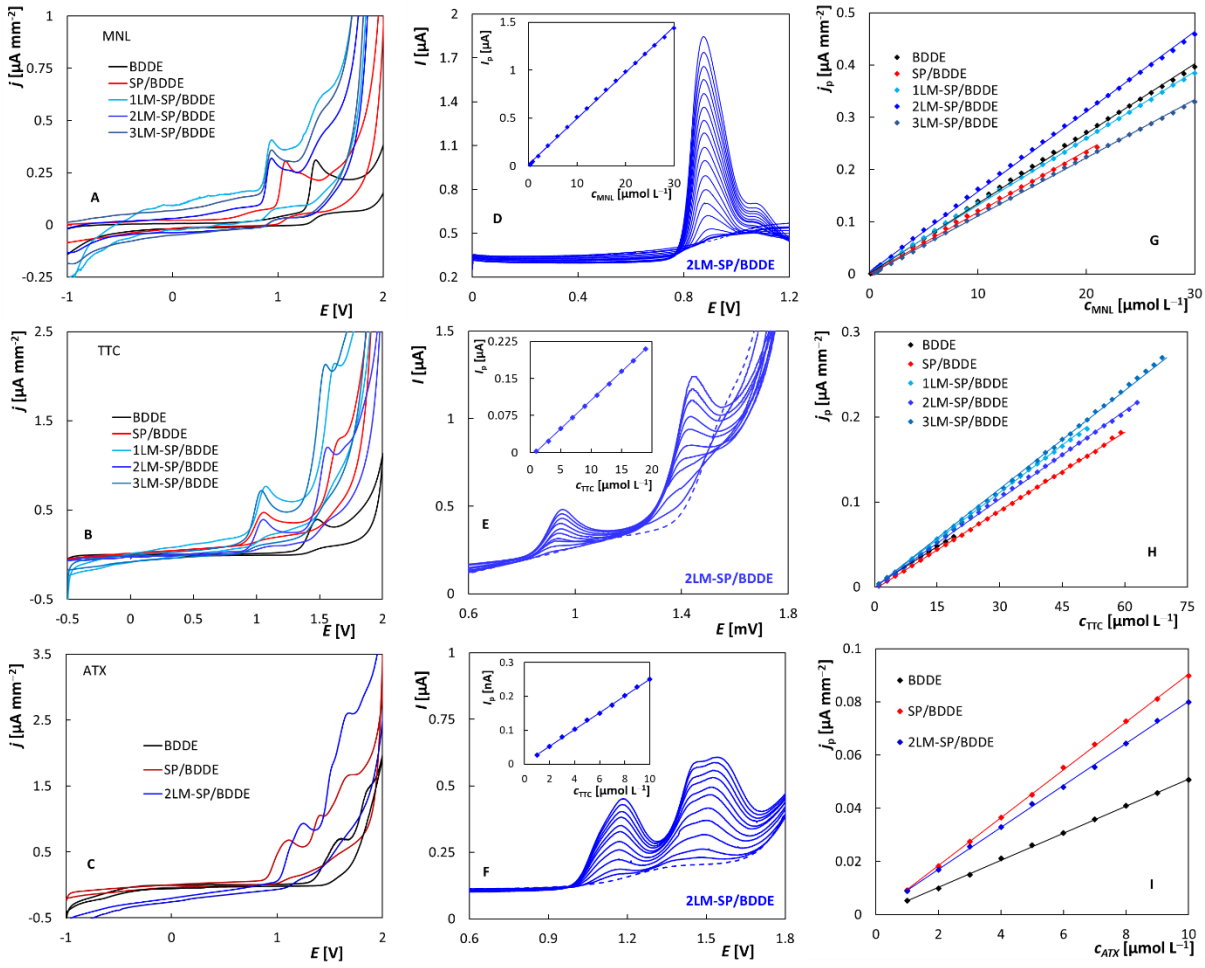

Figure 7 *Cyclic voltammograms of MNL (A), TTC (B) and ATX (C) recorded on all sensors. SW (D, E) and DP (F) voltammograms in dependence on the concentration measured using 2LM-SP/BDDE. Dependence of j_p on concentration of MNL (G), TTC (H) and ATX (I)*

The determination of the investigated substances was performed using SWV and DPV with optimized parameters. Concentration dependencies were measured using the tested sensors, and basic statistical parameters were calculated. An examples of SW/DP

voltammograms for all analyzed substances in dependence on concentration recorded on 2LM-SP/BDDE are shown in Figure 7D-F, and the corresponding dependencies of j_p on c for all tested sensors are shown in Figure 7G-I. Figure 7G presents a comparison in case of MNL, all SPEs provided comparable LDR values as BDDE, except for SP/BDDE, which had limitations at higher concentrations. The lowest LOD and LOQ, identical to BDDE, were provided by 3LM-SP/BDDE. With decreasing electrode surface area, these parameters slightly deteriorated. The results obtained for SP/BDDE were comparable to 1LM-SP/BDDE. In case of TTC, it is evident that the sensitivity is slightly higher for the new LM-SP/BDDE compared to BDDE and SP/BDDE. The LOD values are essentially the same for all tested sensors. SPEs offer significantly broader LDR compared to BDDE. For ATX, it is clear that both SP/BDDE and 2LM-SP/BDDE provide higher slope values than BDDE, but the LOD values for all three sensors were comparable.

Table 2 *Summary of LDR and LOD for the determination of MNL, TTC, ATX*

	LDR [µmol L^{-1}]	**LOD [nmol L^{-1}]**	**LDR [µmol L^{-1}]**	**LOD [nmol L^{-1}]**	**LDR [µmol L^{-1}]**	**LOD [nmol L^{-1}]**
Electrode	**MNL**		**TTC**		**TTC**	
BDDE	0.1-30	55	1-20	250	1-10	160
SP/BDDE	0.3-21	94	1-60	210	1-10	140
1LM-SP/BDDE	0.3-30	99	1-51	280		
2LM-SP/BDDE	0.3-30	74	1-63	180	1-10	130
3LM-SP/BDDE	0.2-30	58	1-70	340		

3.3 Screen-printed sensors with BDDE modified with gold nanoparticles

3.3.1 Surface characterization

SEM images of the unmodified BDD surface and LM-SP/BDDE modified with various types of AuNPs are presented in Figure 8A. The smallest NP size was achieved on the 5Au-SP/BDDE ranging from (16.8±1.7) nm. In the case of a 15 nm Au layer, two NP sizes were observed, with the majority being smaller (25.1±0.8) nm and a minority larger (128.1±5.1) nm. The 50Au-SP/BDDE exhibited NPs with a size of (317.4±24.4) nm. As expected, the size of AuNPs on the electrode surface increased with the growing thickness of the deposited Au layer. The pAu-SP/BDDE yielded NPs with a size of (54.1±1.6) nm, with pores of (6.9±0.2) nm. After ED, NPs with an average diameter of (21.7±0.9) nm were obtained, differing in their crystallographic structure from those obtained by PD, appearing rougher and star-like in shape. The highest NP surface coverage density was achieved after ED. NPs obtained by both presented methods uniformly covered the entire WE`s surface. Raman spectroscopy (Figure 8B) revealed characteristic peaks corresponding to BDD at approximately 460 cm^{-1} (B_1) and 1200 cm^{-1} (B_2), associated with boron incorporation into the diamond structure. The peak at 1290 cm^{-1} (ZCP_D) is related to the diamond structure, and at 1560 cm^{-1} (G), it corresponds to the content of non-diamond carbon, predominantly carbon with sp²

bonding. Surface modification of BDD with AuNPs significantly affected the G peak, indicating an increased content of non-diamond phase. Given that carbon with sp^2 bonding is considered an effective charge transfer center, the increased content of such carbon on the BDD surface may also influence the electrochemical properties of these electrodes.

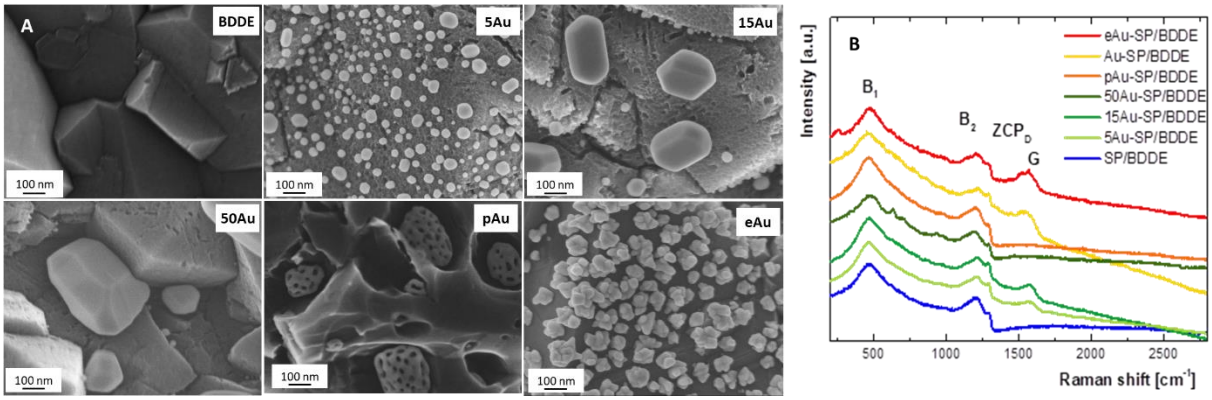

Figure 8 *SEM images of unmodified BDD and BDD modified with AuNPs (magnification 100,000×) (A). Raman spectra of the BDD film taken under excitation at 633 nm (B)*

3.3.2 Electrochemical properties

The electrochemical properties of modified sensors were studied using CV and EIS and compared with unmodified SP/BDDE (referred to as 3LM-SP/BDDE in the previous chapter) and BDDE. Three redox markers, $[Ru(NH_3)_6]^{2+/3+}$, $[Fe(CN)_6]^{4-/3-}$, and DA, were employed. Initially, measurement repeatability was confirmed by conducting ten cyclic voltammograms for all redox markers at a scan rate of 100 mV s^{-1} in 0.1 M KCl for $[Ru(NH_3)_6]^{2+/3+}$ and $[Fe(CN)_6]^{4-/3-}$, and in BRB (pH 5.5) for DA. These results demonstrated excellent repeatability in all cases.

Reversibility of electrochemical reactions was another focus (Figure 9A-C). CV for $[Ru(NH_3)_6]^{2+/3+}$ on different electrodes showed similar current responses, except for Au-SP/BDDE, which exhibited smaller peaks. The I_{pa}/I_{pc} confirmed a reversible reaction (0.9 to 1.3). However, Au-SP/BDDE showed a larger ΔE_p (110.8 mV). The same experiment with $[Fe(CN)_6]^{4-/3-}$ revealed a similar I_{pa}/I_{pc}, suggesting reversibility. The best results were obtained on eAu-SP/BDDE and the worst on BDDE, likely due to AuNPs' catalytic activity. The impact of scan rate on redox markers' curves was investigated. Peak heights increased (I_p) with higher scan rates, linear relationships between I_p and $v^{1/2}$ were obtained, and also logarithmic dependences of I_p on v provided slopes close to the theoretical value of 0.5 typical for a diffusion-controlled reaction.

EIS spectra are shown in Figure 9G-I. In the $[Ru(NH_3)_6]^{2+/3+}$ system, EIS revealed Warburg impedance (diffusion impedance), confirming that $[Ru(NH_3)_6]^{2+/3+}$ behaves as an "*outer sphere*" redox marker unaffected by the electrode surface. For other "*inner sphere*" redox markers like $[Fe(CN)_6]^{4-/3-}$ and DA, which are sensitive to surface quality, EIS provided insights into charge transfer resistance. Most modified electrodes exhibited reduced resistance and increased electron transfer rates, except for those with physically deposited larger gold nanoparticles, which showed slower electron transfer. EIS is a powerful tool for studying analyte and electrode properties when using suitable electrical circuit models. The Maxwell-Wagner effect governs charge relaxation at the

analyte/electrode interface, influencing relaxation time. In summary, modifying BDDE surfaces with gold nanoparticles accelerates electrochemical reactions compared to unmodified diamond and pure gold. Sensors modified via electrochemical deposition of AuNPs exhibited the best electrochemical performance for all tested redox systems.

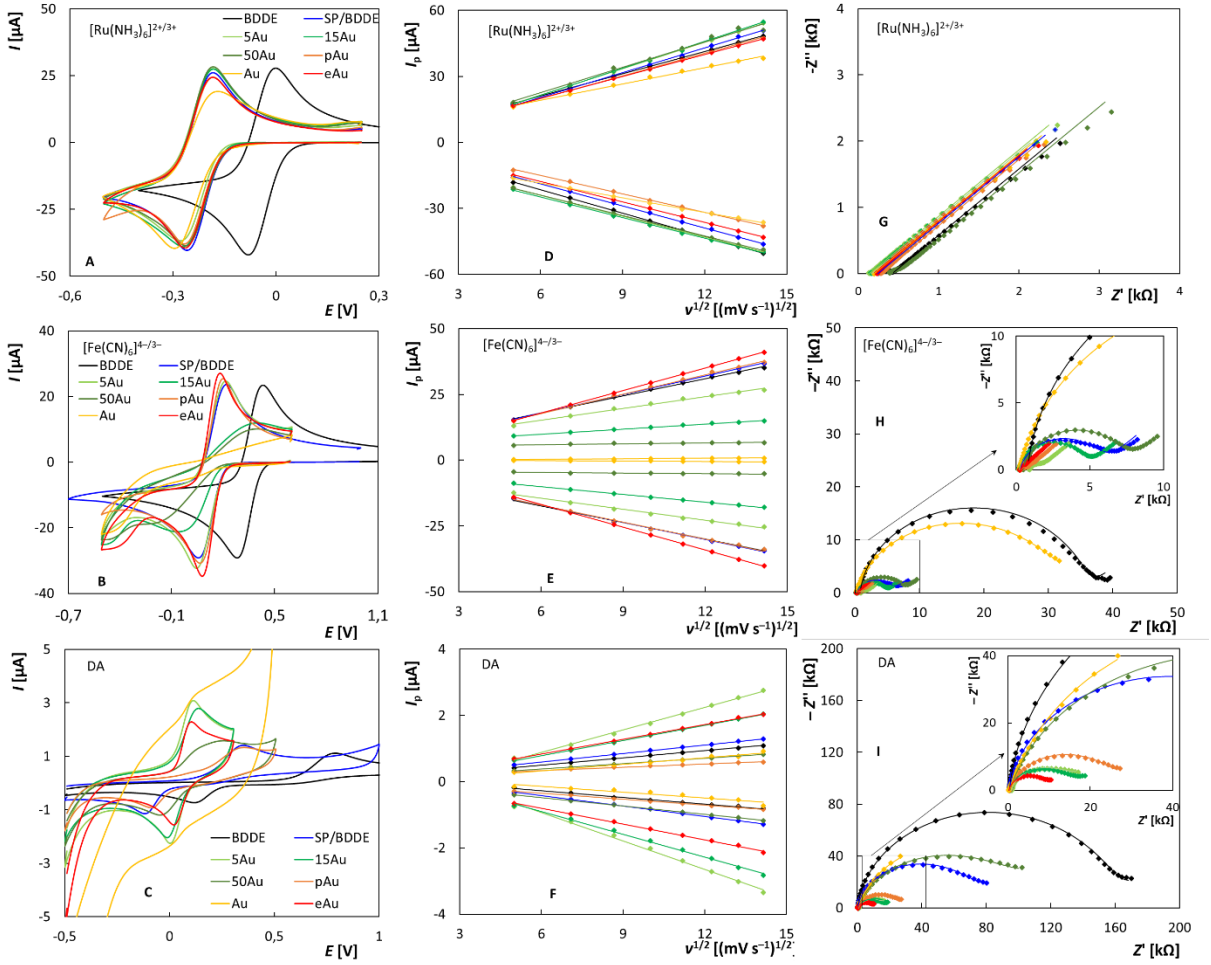

Figure 9 *Cyclic voltammograms of $Ru(NH_3)_6]^{2+/3+}$(A), $[Fe(CN)_6]^{4-/3-}$ (B), and DA (C), dependences $j_p = f(v^{1/2})$ (D-F), and EIS spectra (G-I) recorded on the tested sensors*

3.3.3 Application in electroanalysis

To assess the viability of SP/BDDE modified with AuNPs in electroanalysis, DA was chosen as the model analyte. Initially, the sensors were used to measure I_p dependencies on DA concentration in the range of 1.0 to 15 µmol L^{-1} for determining statistical parameters. The recorded voltammograms with their respective I_p *vs.* c_{DA} dependencies are shown in Figure 10A-H. Notably, the sensor modified through PD with the smallest NPs size (5Au-SP/BDDE) exhibited a substantial increase in the slope (176.8±4.3 nA L µmol^{-1}), marking a 6.5-fold improvement compared to unmodified BDDE or SP/BDDE. Sensitivity decreased as the NPs size increased. Similarly, outstanding results were observed for eAu-SP/BDDE (149.1±1.6 nA L µmol^{-1}). Lowering the v on eAu-SP/BDDE enhanced sensitivity (199.60±0.54 nA L µmol^{-1}). This enhancement can be attributed to the utilization of all electroactive sites, including those within the structured material, at lower scan rates, which remain inactive in redox reactions at higher scan rates. This phenomenon was not observed in sensors with

physically deposited Au (except pAu-SP/BDDE), primarily due to the lower electrode surface coverage density. Moreover, the electrochemically deposited AuNPs have a structured surface, in contrast to the smooth surface resulting from PD. In the case of porous AuNPs, they are embedded deep within the diamond layer, involving the BDD surface in reactions at high scan rates, leading to the formation of two oxidation peaks. After reducing the scan rate, only the first peak corresponding to the reaction on pAuNPs is observed, and its height remains unchanged. In contrast to eAu-SP/BDDE, sensitivity did not increase at lower scan rates for pAu-SP/BDDE, mainly due to the small pore size (approximately 7.0 nm) and the influence of electrocapillary forces.

Concentration dependencies were measured also in a lower concentration range from 0.2 to 1.0 μmol L^{-1} to calculate the LOD. It is evident that the use of new LM-SP/BDDE modified with AuNPs leads to a lower LOD. At the same time, it was found that sensors with smaller NPs, such as 5Au- and 15Au-SP/BDDE or eAu-SP/BDDE (especially at low *v*), provide the best results. Similar LOD values were also obtained for pAu-, although the sensitivity of these sensors (24.5±0.17 nA L μmol^{-1}) was significantly lower. The LOD values achieved in this work for the new sensors modified with AuNPs are the lowest compared to published values in the literature for other types of sensors.

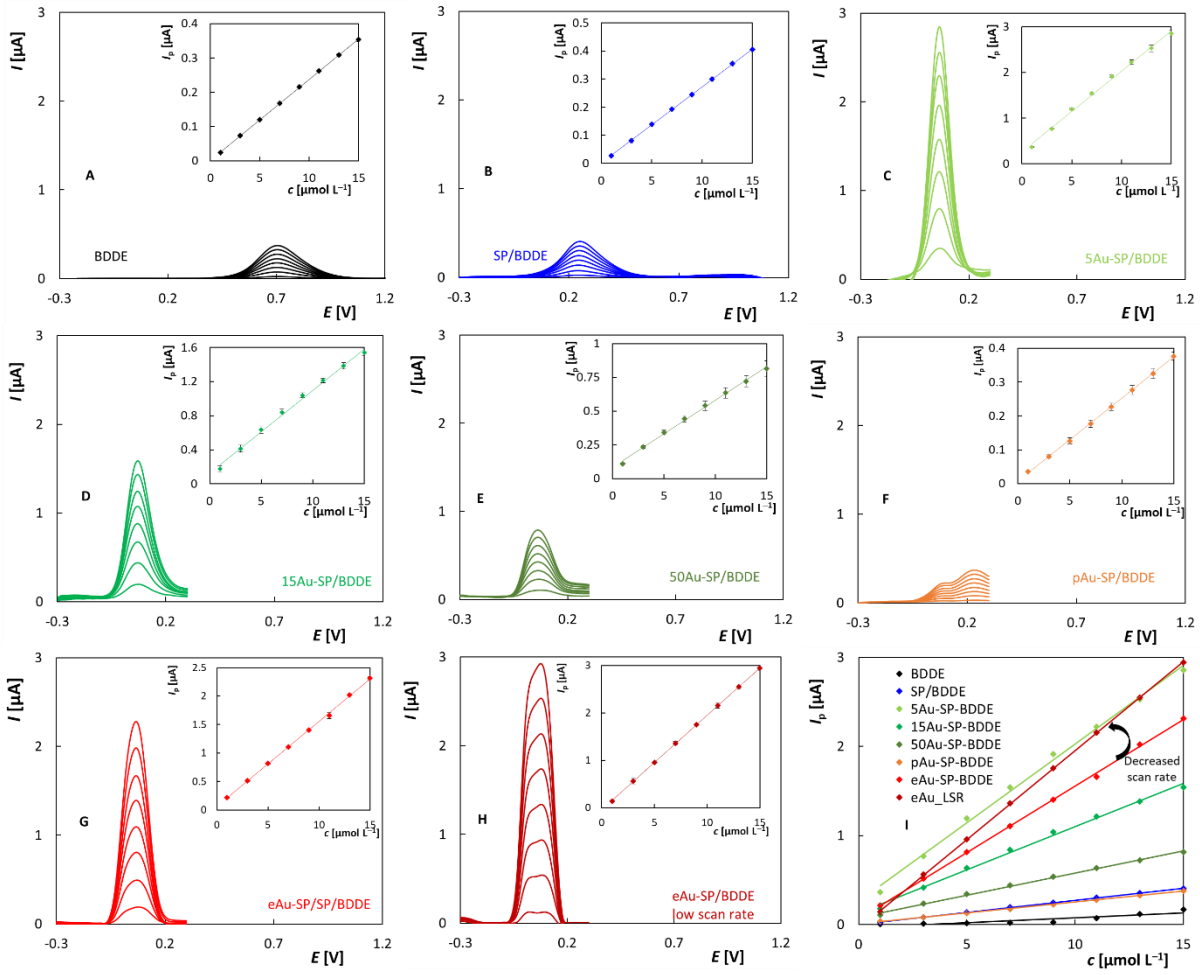

Figure 10 *SW voltammograms of DA depending on the concentration and the corresponding dependence I_p = f(c) (A-H). Concentration dependences obtained for all tested sensors with the added dependence obtained for eAu-SP/BDDE at low scan rate (I)*

Conclusion

In the course of this research, new screen-printed sensors with chemically deposited BDDE were developed, and their physical and electrochemical properties were investigated. Additionally, the possibilities for sensor modification and application in electroanalysis were explored. The initial chapters of the results section focused on the study of the electrochemical behavior and the development of methods for the determination of various biologically active substances relevant to human health and environmental protection. This was done using BDDE in the conventional three-electrode setup of an electrochemical cell. The analyzed substances included pharmaceuticals such as MNL and ATX, the neurotransmitter DA, and the pesticide TTC.

The thesis primarily focused on newly developed LM-SP/BDDE. These sensors were characterized using SEM and Raman spectroscopy, and their electrochemical properties were assessed through CV and EIS with the redox markers $[Fe(CN)_6]^{3-/4-}$ and $[Ru(NH_3)_6]^{3+/2+}$. Comparisons were made with commercially available SP/BDDE and BDDE in conventional setups. The results revealed that the new sensors usually exhibited superior or similar electrochemical properties compared to BDDE. The best performance was observed in 2LM- and 3LM-SP/BDDE, while the commercial SP/BDDE showed the worst outcomes. These new sensors were tested in electroanalysis, demonstrating their effectiveness in real sample analysis. A key advantage of SP sensors is their ability to analyze small sample volumes, with LM-SP/BDDE successfully analyzing a serum sample of 50 μL, whereas SP/BDDE had limitations. Importantly, the study also revealed the termination of production of the tested commercially available SP/BDDE, underlining the significance of the results obtained within this dissertation theses, which provide a high-quality alternative.

In the next phase, new sensors were modified with gold nanoparticles (AuNPs) using a unique physical deposition method. These modified sensors were characterized physically and electrochemically, and their performance in detecting DA was compared to that of LM-SP/BDDE modified with AuNPs via electrochemical deposition and unmodified sensors. It was observed that larger AuNPs were formed with increasing thickness of the deposited Au film. Physically deposited AuNPs had a distinct crystallographic structure and a smoother surface compared to electrochemically prepared ones, which had an irregular, star-like shape. All modified sensors exhibited homogeneous surface coverage, but higher density was achieved through electrochemical deposition. Sensors with smaller AuNPs, such as eAu-SP/BDDE and 5Au-SP/BDDE, demonstrated the best electrochemical properties, possibly due to the catalytic effect of the AuNPs. Increasing NP size resulted in a slower charge transfer rate, as confirmed by EIS. In general, AuNP surface modification improved the electrochemical reactions compared to unmodified BDDE. eAu-SP/BDDE exhibited the lowest charge transfer resistance. When applied in DA analysis, sensors with smaller NPs consistently provided better results, including higher sensitivity and lower LOD values, which are among the lowest values reported in the literature for other sensor types.

In conclusion, the goals set at the beginning of this dissertation have been successfully achieved.

List of citations

1. J. Heyrovský, *Chem. Listy*, 103 (1922) 256–264.
2. J. Barek, F. Opekar, K. Štulík, Elektroanalytická chemie, Karolinum, (2005) Praha.
3. D.S. Austin, J.A. Polta, T.Z. Polta, A.P.-C. Tang, T.D. Cabelka, D.C. Johnson, *J. Electroanal. Chem*, 168 (1984) 227–248.
4. J.B. Benziger, F.A. Pascal, S.L. Bernasek, M.P. Soriaga, A.T. Hubbard, *J. Electroanal. Chem*, 198 (1986) 65–80.
5. J. Zhu, Y. Gong, J. Zhang, P. Shen, H. Chen, *Electroanalysis*, 9 (1997) 1030–1032.
6. S. Baluchová, A. Daňhel, H. Dejmková, V. Ostatná, M. Fojta, K. Schwarzová-Pecková, *Anal. Chim. Acta*, 1077 (2019) 30–66.
7. K.E. Toghill, R.G. Compton, *Electroanalysis*, 22 (2010) 1947–1956.
8. K. Patel, K. Hashimoto, A. Fujishima, *Denki Kagaku1961*, 60 (1992) 659–661.
9. G.M. Swain, Rajeshuni. Ramesham, *Anal. Chem.*, 65 (1993) 345–351.
10. G.M. Swain, A.B. Anderson, J.C. Angus, *MRS Bull.*, 23 (1998) 56–60.
11. C.E. Nebel, J. Ristein, eds., Thin-Film Diamond. II, 1. ed, Elsevier Acad. Press, (2004) Amsterdam.
12. N. Yang, S. Yu, J.V. Macpherson, Y. Einaga, H. Zhao, G. Zhao, G.M. Swain, X. Jiang, *Chem. Soc. Rev.*, 48 (2019) 157–204.
13. K. Schwarzová-Pecková, J. Vosáhlová, J. Barek, I. Šloufová, E. Pavlova, V. Petrák, J. Zavázalová, *Electrochim. Acta*, 243 (2017) 170–182.
14. R. Šelešovská, B. Kränková, M. Štěpánková, P. Martinková, L. Janíková, J. Chýlková, M. Vojs, *J. Electroanal. Chem.*, 821 (2018) 2–9.
15. J. Musilová, J. Barek, K. Pecková, *Chem. Listy*, 103 (2009).
16. V. Hrdlička, O. Matvieiev, T. Navrátil, R. Šelešovská, *Electrochim. Acta*, 456 (2023) 142435.
17. R. Šelešovská, M. Herynková, J. Skopalová, P. Kelíšková-Martinková, L. Janíková, P. Cankař, P. Bednář, J. Chýlková, *Electroanalysis*, 31 (2019) 363–373.
18. R. Šelešovská, F. Hlobeňová, J. Skopalová, P. Cankař, L. Janíková, J. Chýlková, *J. Electroanal. Chem.*, 858 (2020) 113758.
19. K. Muzyka, J. Sun, T.H. Fereja, Y. Lan, W. Zhang, G. Xu, *Anal. Methods*, 11 (2019) 397–414.
20. J. Svítková, Ľ. Švorc, J. Labuda, *Acta Chim. Slov.*, 8 (2015) 172–177.
21. S. Baluchová, A. Mamaloukou, R.H.J.M. Koldenhof, J.G. Buijnsters, *Electrochim. Acta*, 450 (2023) 142238.
22. O. Sarakhman, Ľ. Švorc, *Crit. Rev. Anal. Chem.*, 52 (2022) 791–813.
23. A. Usenko, J. Chýlková, R. Šelešovská, M. Sedlák, J. Váňa, J. Bartáček, T. Mikysek, *J. Electroanal. Chem.*, 904 (2022) 115857.
24. A. Usenko, J. Chýlková, J. Váňa, O. Matvieiev, L. Janíková, R. Šelešovská, *J. Electroanal. Chem.*, 935 (2023) 117360.
25. G. Kuchtová, J. Chýlková, J. Váňa, M. Vojs, L. Dušek, *J. Electroanal. Chem.*, 863 (2020) 114036.
26. G. Kuchtová, L. Hojová, A.V. Staňová, M. Marton, M. Vrška, M. Behúl, P. Michniak, M. Vojs, L. Dušek, *Electrochim. Acta*, 464 (2023) 142924.
27. M. Li, Y.-T. Li, D.-W. Li, Y.-T. Long, *Anal. Chim. Acta*, 734 (2012) 31–44.
28. Z. Taleat, A. Khoshroo, M. Mazloum-Ardakani, *Microchim. Acta*, 181 (2014) 865–891.
29. J. Barton, M.B.G. García, D.H. Santos, P. Fanjul-Bolado, A. Ribotti, M. McCaul, D. Diamond, P. Magni, *Microchim. Acta*, 183 (2016) 503–517.
30. H. Beitollahi, S.Z. Mohammadi, M. Safaei, S. Tajik, *Anal. Methods*, 12 (2020) 1547–1560.

31. M. Pohanka, *Int. J. Electrochem. Sci.* (2020) 11024–11035.
32. P. Kelíšková, O. Matvieiev, L. Janíková, R. Šelešovská, *Curr. Opin. Electrochem.*, 42 (2023) 101408.
33. Z. Liu, S. Baluchová, B. Brocken, E. Ahmed, P. Pobedinskas, K. Haenen, J.G. Buijnsters, *ACS Appl. Mater. Interfaces*, 15 (2023) 39915–39925.
34. S. Đurđić, F. Vlahović, M. Markićević, J. Mutić, D. Manojlović, V. Stanković, Ľ. Švorc, D. Stanković, *Chemosensors*, 11 (2023) 15.
35. D.M. Stanković, Z. Milanović, Ľ. Švorc, V. Stanković, D. Janković, M. Mirković, S.V. Đurić, *Diam. Relat. Mater.*, 113 (2021) 108277.
36. O. Sarakhman, A. Benková, Ľ. Švorc, *Microchem. J.*, 175 (2022) 107132.
37. K.-F. Benitz, R. Moraski, R.R. Roepke, L.A. Wozniak, *Toxicol. Appl. Pharmacol.*, 4 (1962) 220–237.
38. I.A. Kraft, *Am. J. Psychiatry*, 118 (1962) 841–842.
39. N. Erk, *J. Pharm. Biomed. Anal*, 21 (1999) 429–437.
40. A.A. Bredikhin, Z.A. Bredikhina, D.V. Zakharychev, A.V. Pashagin, *Tetrahedron: Asymmetry*, 18 (2007) 1239–1244.
41. P. Lowinger, *Am. J. Psychiatry*, 120 (1963) 66–67.
42. A. Ochoa-Terán, I.A. Rivero, *Arkivoc.*, 2008 (2008) 235–242.
43. J. Dohnal, Z. Volková, K. Vytřas, *J. Pharm. Biomed. Anal*, 7 (1989) 755–758.
44. G.D. Laveck, P. Bwkley, *J. Chronic. Dis.*, 13 (1960) 174–183.
45. J. Eskenazi, T. Nikiforidis, J.J. Livio, J.L. Schelling, *Eur. J. Clin. Pharmacol.*, 9 (1976) 411–415.
46. B.V. Franko, J.W. Ward, D.L. Gilbert, G. Woodard, *Toxicol. Appl. Pharmacol.*, 19 (1971) 93–102.
47. R.A. Yeary, R.A. Benish, C.A. Brahm, D.L. Miller, *Toxicol. Appl. Pharmacol.*, 6 (1964) 642–652.
48. G. Yu, G.-F. Li, J.S. Markowitz, *J. Child Adolesc. Psychopharmacol.*, 26 (2016) 314–326.
49. J. Biederman, S.V. Faraone, *The Lancet*, 366 (2005) 237–248.
50. J.D.D. Bradley, C.J. Golden, *Clin. Psychol. Rev.*, 21 (2001) 907–929.
51. F. Bymaster, *Neuropsychopharmacology*, 27 (2002) 699–711.
52. M. Pérez-Ortiz, C. Muñoz, C. Zapata-Urzúa, A. Álvarez-Lueje, *Talanta*, 82 (2010) 398–403.
53. H. Lund, O. Hammerich, eds., Organic Electrochemistry, 4th Edition, Marcel Decker, (2001).
54. European Centre for Disease Prevention and Control., Risk Assessment on the Impact of Environmental Usage of Traizoles on the Development and Spread of Resistance to Medical Triazoles in Aspergillus Species., Publications Office, (2013) LU.
55. M. Jakl, I. Kovač, S. Ćavar Zeljković, J. Jaklová Dytrtová, *Food Chemistry*, 351 (2021) 129328.
56. BASF SE Grop Protection Division, *Https://Agriculture.Basf.Com* (2015).
57. D.P. Biradar, W.L. Pedersen, A.L. Rayburn, *Pestic. Sci.*, 41 (1994) 291–295.
58. M.-P. Charnay, C. Verge, E. Barriuso, *Pest Manag Sci* (2000) 8.
59. J.-B. Speakman, R. Stierl, S. Strathmann, P. Dombo, M. Niedenbrueck, E. Haden, D. Voeste, D. Groeger, Method for Controlling Mycoses in Leguminous Plants, EP20050817599, 2005.
60. C. Beigel, M.-P. Charnay, E. Barriuso, *Soil Biol. Biochem.*, 31 (1999) 525–534.
61. C. Beigel, E. Barriuso, L. Di Pietro, *J. Environ. Qual.*, 26 (1997) 1503–1510.
62. M. Jakl, J. Fanfrlík, J. Jaklová Dytrtová, *Rapid Commun. Mass Spectrom.*, 31 (2017) 2043–2050.

63. J. Jaklová Dytrtová, K. Bělonožníková, M. Jakl, H. Ryšlavá, *Environ. Pollut.*, 266 (2020) 115201.
64. L. Cruickshank, A.R. Kennedy, N. Shankland, *J. Mol. Struct.* (2013).
65. R. Horowski, P.-A. Löschmann, *J. Neural. Transm.*, 126 (2019) 449–454.
66. S.D. Iversen, L.L. Iversen, *Trends Neurosci.*, 30 (2007) 188–193.
67. W. Dauer, S. Przedborski, *Neuron*, 39 (2003) 889–909.
68. A. Teniou, A. Rhouati, G. Catanante, *Appl. Biochem. Biotechnol.*, 194 (2022) 1925–1937.
69. J. Breczko, M.E. Plonska-Brzezinska, L. Echegoyen, *Electrochim. Acta*, 72 (2012) 61–67.
70. D. Wang, P. Schaaf, *J. Mater. Chem.*, 22 (2012) 5344.
71. K. Pungjunun, S. Chaiyo, I. Jantrahong, S. Nantaphol, W. Siangproh, O. Chailapakul, *Microchim. Acta*, 185 (2018) 324.
72. W.T. Wahyuni, T.A. Ivandini, P.K. Jiwanti, E. Saepudin, J. Gunlazuardi, Y. Einaga, *Electrochemistry*, 83 (2015) 357–362.
73. F. Bottari, K. De Wael, *J. Electroanal. Chem.*, 801 (2017) 521–526.
74. S. Szunerits, R. Boukherroub, *C. R. Chim.*, 11 (2008) 1004–1009.
75. J.W. Strojek, M.C. Granger, G.M. Swain, T. Dallas, M.W. Holtz, *Anal. Chem.*, 68 (1996) 2031–2037.
76. M.C. Granger, G.M. Swain, *J. Electrochem. Soc.*, 146 (1999) 4551–4558.
77. F. Friso, S. Trasatti, *Collect. Czech. Chem. Commun.*, 68 (2003) 1621–1635.
78. Shokoofeh. Alehashem, Fred. Chambers, J.W. Strojek, G.M. Swain, Rajeshuni. Ramesham, *Anal. Chem.*, 67 (1995) 2812–2821.
79. S. Ferro, A. De Battisti, *Electrochim. Acta*, 47 (2002) 1641–1649.
80. J. Mocak, A.M. Bond, S. Mitchell, G. Scollary, *Pure Appl. Chem.*, 69 (1997) 297–328.
81. R.S. Nicholson, *Anal. Chem.*, 37 (1965) 1351–1355.
82. M.M. Al-Kassab, A.H. Majeed, *ADAS*, 81 (2022) 13–22.
83. F. Pruvost, A. Deneuville, *Diam. Relat. Mater.*, 10 (2001) 531–535.
84. M. Marton, M. Vojs, E. Zdravecká, M. Himmerlich, T. Haensel, S. Krischok, M. Kotlár, P. Michniak, M. Veselý, R. Redhammer, *J. Spectrosc.*, 2013 (2013) 1–6.
85. J.V. Macpherson, *Phys. Chem. Chem. Phys.*, 17 (2015) 2935–2949.
86. S.C. B. Oliveira, A.M. Oliveira-Brett, *Electrochim. Acta*, 55 (2010) 4599–4605.

List of Student's Published Works

Articles on the topic of the dissertation theses

HRDLIČKA, Vojtěch, MATVIEIEV, Oleksandr, NAVRÁTIL, Tomáš, ŠELEŠOVSKÁ, Renáta. Recent advances in modified boron-doped diamond electrodes: A review. *Electrochimica Acta*, 2023, 456, 142435.

MATVIEIEV, Oleksandr., ŠELEŠOVSKÁ, Renáta, SOKOLOVÁ, Romana, JERGA, Radek, SKOPALOVÁ, Jana, BARTÁK, Petr, CHÝLKOVÁ, Jaromíra, VOJS, Marian. Voltammetric analysis of mephenoxalone drug in pharmaceutical and biological samples using novel screen-printed sensor with boron-doped diamond electrode. *Sensors and Actuators B: Chemical*, 2023, 397, 134700.

ŠELEŠOVSKÁ, Renáta, NAVRÁTIL, Tomáš, HRDLIČKA, Vojtěch, MICHNIAK, Pavol, HATALA, Michal, VOJS, Marian, MARTON, Marián, MATVIEIEV, Oleksandr, JANÍKOVÁ, Lenka, CHÝLKOVÁ, Jaromíra. Novel screen-printed sensors with chemically deposited boron-doped diamond and their use for voltammetric determination of attention deficit hyperactivity disorder medication atomoxetine. *Electrochimica Acta*, 2022, 403, 139642.

MATVIEIEV, Oleksandr, ŠELEŠOVSKÁ, Renáta, VOJS, Marian, MARTON, Marián, MICHNIAK, Pavol, HRDLIČKA, Vojtěch, HATALA, Michal, JANÍKOVÁ, Lenka, CHÝLKOVÁ, Jaromíra, SKOPALOVÁ, Jana, CANKAŘ, Petr, NAVRÁTIL, Tomáš. Novel screen-printed sensor with chemically deposited boron-doped diamond electrode: preparation, characterization, and application. *Biosensors*, 2022, 12, 241.

MATVIEIEV, Oleksandr, ŠELEŠOVSKÁ, Renáta, MARTON, Marián, HATALA, Michal, METELKA, Radovan, WEIS, Martin, VOJS, Marian. Effect of different modification by gold nanoparticles on the electrochemical performance of screen-printed sensors with boron-doped diamond electrode. *Scientific Reports*, 2023, 13, 21525.

Next articles

ŠELEŠOVSKÁ, Renáta, SOKOLOVÁ, Romana, KREJČOVÁ, Kateřina, SCHWARZOVÁ-PECKOVÁ, Karolina, MIKYSEK, Tomáš, MATVIEIEV, Oleksandr. Electrochemical behavior of fungicide tebuconazole and its voltammetric determination on an oxygen-terminated boron-doped diamond electrode. *Journal of Electroanalytical Chemistry*, 2023, 930, 117155.

USENKO, Alona, CHÝLKOVÁ, Jaromíra, VÁŇA, Jiři, MATVIEIEV, Oleksandr, JANÍKOVÁ, Lenka, ŠELEŠOVSKÁ, Renáta. A new voltammetric approach for the determination of the growth retardant paclobutrazol in the presence of difenoconazole in pesticide preparations. *Journal of Electroanalytical Chemistry, 2023*, 935, 117360.

KELÍŠKOVÁ, Pavlína, MATVIEIEV, Oleksandr, JANÍKOVÁ, Lenka, ŠELEŠOVSKÁ, Renáta. Recent advances in the use of screen-printed electrodes in drug analysis: A review. *Current Opinion in Electrochemistry*, 2023, 42, 101408.